Alternating Flow Model for Mass and Heat Dispersion in Packed Beds

The alternating flow model (AFM) views dispersion in packed beds as a sequence of streamline plugs that must repeatedly split and merge as the bulk fluid traverses the vessel. Thus, the flow in the AFM is ordered, as opposed to the random flow implied by the Fickian analogy. For mass dispersion only, model parameters arise from *a priori* considerations of packing geometry. Steady state and transient data ($5.6 < D_t/d_p < 54.4$, $100 < Re_p < 1{,}000$, gases and liquids) show the AFM to surpass the Fickian analogy (based on correlations for dispersion coefficients) in most cases. Further, it can describe well the radial velocity profile trends in packed beds. For heat dispersion, two additional parameters (heat transfer coefficients) arise that are not functions of packing geometry. Simple correlations for these parameters and the justifications are given. Most of the comparisons made with the literature experimental results show the AFM to be at least as good as the back-fit Fickian analogy. The AFM should be most useful for packed beds with a relatively small D_t/d_p.

K. J. Klingman, H. H. Lee
Department of Chemical Engineering
University of Florida
Gainesville, FL 32611

Introduction

Dispersion in packed beds has traditionally been modeled by analogy to Fickian diffusion, e.g., for a constant-density fluid

$$\frac{\partial C}{\partial t} + U\frac{\partial C}{\partial z} - Da\frac{\partial^2 C}{\partial z^2} - Dr\frac{1}{r}\frac{\partial}{\partial r}\left(r\frac{\partial C}{\partial r}\right) = 0 \qquad (1)$$

where the axial and radial dispersion coefficients Da and Dr are effective parameters that account for the presence of packing material. The usual procedure for modeling packed beds is to obtain the dispersion coefficients and then to solve Eq. 1 either analytically or numerically for the appropriate boundary conditions.

An acceptable dispersion model should at the very least adequately describe the simplest problem of injecting nonreacting dye into a clear stream flowing through a bed packed with nonporous beads. The solution of Eq. 1 for the simple dye injection problem predicts backmixing in the region of Reynolds number (Hiby, 1963) where none is observed experimentally.

Mixing-cell models (Deans and Lapidus, 1960) overcome the backmixing problem but predict that concentration wavefronts travel at infinite speed, i.e., any change in inlet concentration is immediately seen at the bed outlet. Experimental observations (Sundaresan et al., 1980) indicate that concentration propagates at a finite speed. Also, no standard technique for sizing the individual mixing cells is available.

Other researchers have also proposed stochastic (Schmalzer and Hoelscher, 1971), capillary (Lippert and Schneider, 1979), and probabilistic time-delay models (Buffham, 1971), and crossflow models (Hinduja, 1977; Hinduja et al., 1980) for packed beds. In addition, the literature provides several reviews of and cautions regarding packed-bed models (Aris and Amundson, 1957; Gunn, 1969; Levenspiel and Fitzgerald, 1983; Vortmeyer and Winter, 1984).

What then are the characteristics of an acceptable packed-bed dispersion model? The model should provide the correct steady state form (axial and radial spreading, no backmixing, agreement with experimental data) and should predict the correct transient behavior (finite speed of propagation, conservation system) (Sundaresan et al., 1980). The model should also properly represent the flow around packing; its solution, analytical or numerical, should be straightforward; and its corresponding parameters should be well defined. None of the currently available models meets all the acceptability criteria.

The objectives here are to present a model that describes the flow in packed beds as a series of alternating annular plugs, the so-called alternating flow model (AFM), and then to develop

Correspondence concerning this paper should be addressed to H. H. Lee.

the corresponding mathematical model. Mass dispersion is considered first. The mass dispersion results are then extended to heat dispersion.

Concept and Qualitative Support for AFM

The basic question that can be raised in applying the Fickian analogy to a packed bed is whether the underlying assumption of randomness implied by Fick's law is still valid in light of the fact that the Fickian analogy works well at least at small Reynolds number for empty tubes, but presents difficulties when applied to packed beds. It is of interest in this regard that if a particle exhibits random motion, with no preference for direction of travel, as it traverses the length of the vessel, then statistical analysis will lead to Eq. 1 (Baron, 1952; Jacques and Vermeulen, 1957). The question then arises as to whether the presence of packing within the tube would impose some order to the flow.

Gunn and Pryce (1969) carried out several experiments in packed beds of two types, one with the packing intentionally arranged in a regular pattern and another with random (dumped) packing. Their analysis showed that the Fickian dispersion parameters could not be fitted to the regular array case, but that the Fickian parameters did fit the random-packing case. This lends support to the idea that Eq. 1 may not adequately describe conditions of nonrandom motion.

In addition, other researchers (Hiby, 1963; Bischoff and McCracken, 1966; Kubo et al., 1979) experimented with time-lapse photography to observe the flow patterns around pellets in packed beds. Patterns such as those shown schematically in Figure 1 were consistently observed. The experiment illustrated in Figure 1 is for flow around cylinders between two flat plates. This streamline split-merge pattern did not break down even as the velocity was increased by two orders of magnitude (Hiby, 1963). This lends support to the idea that the packing arrangement dominates the actual fluid velocity in determining mixing characteristics within packed beds.

How, then, is it possible to use this information to aid the description of dispersion in packed beds? If one draws a vertical axis through the middle of the flat plates illustrated by Figure 1 and then rotates these plates about that axis, the rotation paths made by the void and occupied channels could be viewed as void and occupied annuli as shown in Figure 2. As the fluid flows through this sequence of void-full annular cells it alternately splits and merges; hence, the name alternating flow model. The basic premise of this paper, then, is that this AFM approximation, developed solely from observations of packed-bed flow behavior, accurately describes not only the flow, but also the dispersion behavior in packed beds. Further, the resulting equations can be solved in a straightforward manner and the corresponding physical parameters can be determined *a priori*, as opposed to being back-fitted to laboratory data.

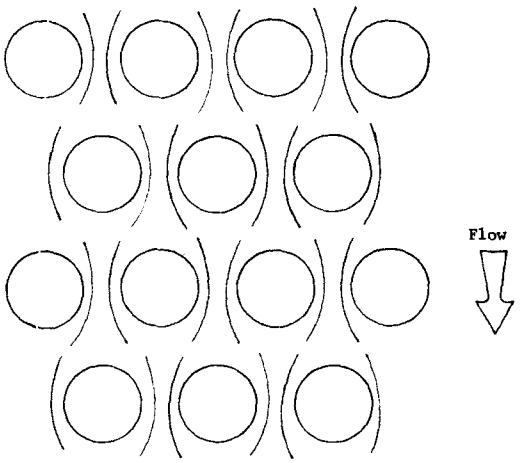

Figure 1. Flow patterns in packed beds.

Alternating Flow Model Development (Mass Dispersion)

The alternating flow model presumes that flow through a packed bed can be described by an axially repeating series of cells, the repeating cell being the one in Figure 2, and that the fluid moving through each void space exhibits plug flow behavior. Thus, dispersion is achieved by repeated splitting and merging of these fluid plugs as the bulk fluid traverses the length of the bed.

If a cylindrical tube is packed with inert, uniformly sized spheres, the simplest mass dispersion cases are the steady state injection of dye, or tracer, on the tube axis and a transient step change in concentration across the entire inlet cross section. For these cases, two AFM parameters define the dispersion behavior: the number (size) and distribution of radial plugs within each A or B half-cell, and the length of each repeating A/B cell, Figure 2. The distribution of the flow among the individual radial plugs, or the split-merge behavior, follows from these dimensions via a hydraulic resistance argument.

Consider as an example a tube divided into six concentric annuli as shown in Figure 2. Since the flow into a channel of arbitrary cross section is described by

$$\Delta P = \frac{U^2 f \rho (L/R_h)}{2g_c} \tag{2}$$

and

$$f = \begin{cases} \text{const}/Re & \text{laminar} \\ \text{const} & \text{turbulent} \end{cases} \tag{3}$$

the total flow Q_t entering a pipe of pattern A, Figure 2, will be distributed to each plug (void section) as

$$Q_i/Q_t = \frac{1}{H_i} \Big/ \sum_1 \left(\frac{1}{H_i}\right) \quad i = 2, 4, 6 \tag{4}$$

Here, R_h is the hydraulic radius (cross-sectional area/wetted perimeter), L is the plug length, U is the fluid velocity, g_c is the gravity units conversion factor, and ΔP is the pressure drop over the length L. In the above relationship, the individual hydraulic resistance, H_i, depends on annulus dimensions and on flow regime (Klingman, 1985) as follows:

$$\frac{1}{H_i} = \begin{cases} \beta A R_h^2 & \text{laminar} \\ \beta A (R_h)^{1/2} & \text{turbulent} \end{cases} \tag{5}$$

where β is a proportionality constant and A is the annulus cross-sectional area. The distinction between laminar and turbulent

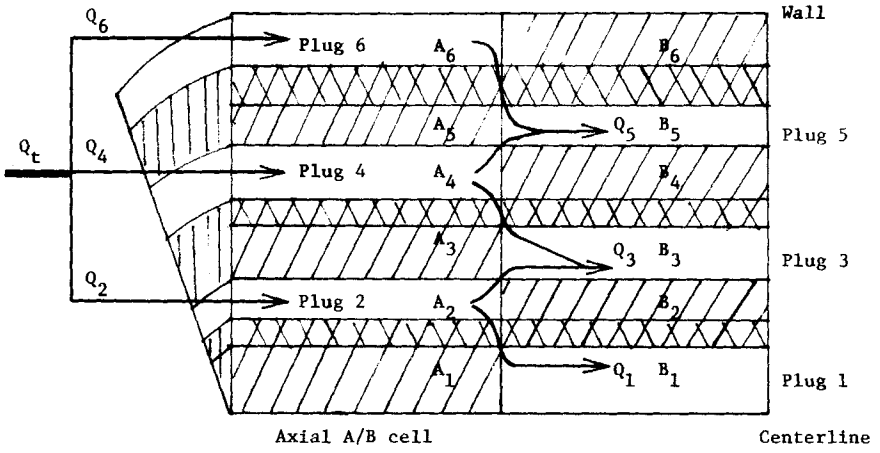

Figure 2. One AFM repeating *A/B* cell, $N_{rad} = 6$.

flow is based on the particle Reynolds number, $(Re)_p$, with the pellet diameter as the length scale, for flow around individual spheres; $(Re)_p > 150$ for turbulence and $(Re)_p < 150$ for laminar flow. It is noted in this regard that the flow distribution in accordance with the Ergun-type resistances is essentially the same as that given by Eq. 5 (Klingman, 1985). As the fluid flows from the A half-cell to the B half-cell, Figure 2, the plug 2 flow splits in proportion to the hydraulic resistances presented by plugs 1 and 3, the plug 4 flow splits in proportion to the plug 3 and 5 resistances, and the plug 6 flow must all enter plug 5, i.e.,

$$
\begin{aligned}
&Q_1/Q_t = (1 - W_3)Q_2/Q_t \\
&Q_3/Q_t = [W_3Q_2 + (1 - W_5)Q_4]/Q_t \\
&Q_i/Q_t = [W_iQ_{i-1} + (1 - W_{i+2})Q_{i+1}]/Q_t \\
&\qquad \text{for } i = 3, 5, \ldots, N - 3 \\
&Q_5/Q_t = (W_5Q_4 + Q_6)/Q_t;\ Q_i/Q_t = (W_iQ_{i-1} + Q_{i+1})/Q_t \\
&\qquad \text{for } i = N - 1
\end{aligned} \tag{6}
$$

where N is the total number of the void radial plugs in a cell. The individual weighting factors W_i are determined by the resistance of those B plugs into which each A plug must split. Consider, for example, A plug 4 as it splits via two competing resistances into B plugs 3 and 5 (just as there were three competing resistances for the total flow entering the pattern A). Then

$$
\begin{aligned}
Q_5/Q_4 &= \frac{1/H_5}{1/H_3 + 1/H_5} = W_5 \\
Q_3/Q_4 &= \frac{1/H_3}{1/H_3 + 1/H_5} = 1 - W_5
\end{aligned} \tag{7}
$$

Hence, the weighting factors in Eq. 6 are given by

$$
W_i = \frac{1/H_i}{1/H_i + 1/H_{i-2}} \tag{8}
$$

where the subscripts are as illustrated in Figure 2 and the hydraulic resistances are defined in Eq. 5. As the fluid moves from the B half-cell into the next A half-cell, the plugs recombine in such a way as to regain the original A distribution. This means that the concentration entering each plug is a weighted average of the outlets of preceding plugs, Figure 2:

A to B transition:

$$
\begin{aligned}
C_1 &= C_2 \\
C_3 &= [(1 - W_5)Q_4C_4 + W_3Q_2C_2]/Q_3 \\
C_5 &= (W_5Q_4C_4 + Q_6C_6)/Q_5
\end{aligned} \tag{9a}
$$

B to A transition:

$$
\begin{aligned}
C_2 &= W_3C_3 + (1 - W_3)C_1 \\
C_4 &= W_5C_5 + (1 - W_5)C_3 \\
C_6 &= C_5
\end{aligned} \tag{9b}
$$

Here, W_i can be viewed as the fraction of the flow from A plug $(i - 1)$ to B plug i. Note in the B to A transition that the plugs recombine simply to regain the original A distribution.

Consider simple mass dispersion with no reaction. The plug flow equation for each radial plug is

$$
\frac{\partial C}{\partial t} + U\frac{\partial C}{\partial z} = 0 \tag{10}
$$

(determination of the individual linear velocities U is discussed below). The solution of Eq. 10 indicates that the concentration at the outlet of each radial plug is simply its input signal delayed by a dead time equal to the half-cell length divided by U. Since the fluid must transverse a series of delays before exiting the bed, a finite time will pass before any inlet changes will propagate to the outlet.

In the steady state case, the outlet and inlet concentrations of any plug are equal, and the concentration profile at the nth axial cell can be determined from the inlet profile:

$$
\boldsymbol{A}_n = (\boldsymbol{SR})^{n-1}\boldsymbol{C}_{in} \quad n = 1, 2, 3, \ldots, N_{axial} \tag{11}
$$

$$
\boldsymbol{B}_n = \boldsymbol{RA}_n \tag{12}
$$

where

$$\boldsymbol{A}_n^T = [(C_2)_n, (C_4)_n, (C_6)_n \ldots, (C_{2m})_n, \ldots] \tag{13}$$

$$\boldsymbol{B}_n^T = [(C_1)_n, (C_3)_n, (C_5)_n, \ldots, (C_{2m+1})_n, \ldots]$$

Here, $\boldsymbol{A}$ is the concentration vector for the radial void plugs in the A half-cell in Figure 2, $\boldsymbol{B}$ is the same in the B half-cell, n is the index for the A/B axial cell numbered from the tube inlet such that n is zero for the inlet, and N_{axial} is the total number of A/B axial cells. Thus, $(C_4)_n$, for instance, is the concentration of A plug 4 in the nth axial cell. The number of elements in each of A and B half-cells is K, and therefore the total number of void radial plugs in an A/B cell is $2K$. The di-diagonal matrices $\boldsymbol{S}$ and $\boldsymbol{R}$ are such that the matrix elements are given by

$$s_{i,i} = \begin{cases} 1 - W_{2i+1} & i = 1, 2, 3, \ldots, [(N/2) - 1] \\ 1 & i = (N/2) \end{cases}$$

$$s_{i,i+1} = \begin{cases} W_{2i+1} & i = 1, 2, 3, \ldots, [(N/2) - 1] \\ 0 & i = (N/2) \end{cases} \tag{14}$$

$$r_{i,i} = \begin{cases} 1 & i = 1 \\ \dfrac{(1 - W_{2i+1})Q_{2i}}{Q_{2i-1}} & i = 2, 3, \ldots, N/2 \\ Q_N/Q_{N-1} & i = N/2 \end{cases}$$

$$r_{i,i-1} = \begin{cases} 0 & i = 1 \\ \dfrac{W_{2i-1}Q_{2i-2}}{Q_{2i-1}} & i = 2, 3, \ldots, N/2 \end{cases} \tag{15}$$

Equations 11 and 12 follow from the following facts:

$$\boldsymbol{B}_n = \boldsymbol{R}\boldsymbol{A}_{n-1} \tag{16}$$

$$\boldsymbol{A}_n = \boldsymbol{S}\boldsymbol{B}_n = \boldsymbol{S}\boldsymbol{R}\boldsymbol{A}_{n-1}; \boldsymbol{A}_0 = \boldsymbol{C}_{in} \tag{17}$$

which follow from the mixing pattern given in Figure 2. Equation 9a is Eq. 16 written for $n = 1$ and $N = 6$; Eq. 9b is Eq. 17 written for $n = 1$ and $N = 6$. Note that a point source of dye is simulated by setting $(C_2)_{in} = C_{in}$ and $(C_4)_{in} = (C_6)_{in} = \cdots = (C_{2_m})_{in} = 0$. Since the concentration in any given radial plug is solely a function of upstream conditions, no backmixing is predicted.

In the transient case, it is more convenient to treat the dead times in the Laplace domain. A uniform step change in inlet concentration is simulated by setting all elements of $\boldsymbol{A}_0$ equal to C_{in}/s. Since the outlet concentration of any plug is the inlet concentration delayed by the dead time, one has for any plug

$$\boldsymbol{A}_{out} = \boldsymbol{\theta}_A\boldsymbol{A}_{in} \tag{18}$$

$$\boldsymbol{B}_{out} = \boldsymbol{\theta}_B\boldsymbol{B}_{in} \tag{19}$$

where $\boldsymbol{\theta}_A$ and $\boldsymbol{\theta}_B$ are diagonal matrices whose diagonal elements are given by

$$(\theta_A)_{i,i} = \exp(-sd_i); d_i = (Z_c/2)/U_{2i} \quad i = 1, 2, \ldots, K$$
$$(\theta_B)_{j,j} = \exp(-sd_j); d_j = (Z_c/2)/U_{(2i-1)} \quad j = 1, 2, \ldots, K \tag{20}$$

Here, Z_c is the length of the axial A/B cell, the subscripts *in* and *out* are for the inlet and outlet of any given radial plug, and s is the Laplace transform variable. The equations corresponding to Eqs. 11 and 12 are:

$$(\boldsymbol{A}_{in})_n = \boldsymbol{S}(\boldsymbol{B}_{out})_{n-1} = \boldsymbol{S}\boldsymbol{\theta}_B(\boldsymbol{B}_{in})_{n-1} \tag{21}$$

$$(\boldsymbol{B}_{in})_n = \boldsymbol{R}(\boldsymbol{A}_{out})_n = \boldsymbol{R}\boldsymbol{\theta}_A(\boldsymbol{A}_{in})_n \tag{22}$$

where Eqs. 18 and 19 have been used. It follows from Eqs. 21 and 22 that

$$(\boldsymbol{A}_{in})_n = (\boldsymbol{S}\boldsymbol{\theta}_B\boldsymbol{R}\boldsymbol{\theta}_A)^{n-1}C_{in}/s \tag{23}$$

$$(\boldsymbol{B}_{out})_n = \boldsymbol{\theta}_B\boldsymbol{R}\boldsymbol{\theta}_A(\boldsymbol{S}\boldsymbol{\theta}_B\boldsymbol{R}\boldsymbol{\theta}_A)^{n-1}C_{in}/s \tag{24}$$

Note that Eqs. 23 and 24 imply a radial distribution of the total time delay required for an inlet change to be seen at the outlet, i.e., a residence time distribution. The matrix formulation for the transient case was to concisely represent and account for the radial and axial distribution of delay times. In concept, the simulation is straightforward, but it does require some careful bookkeeping at the actual computer programming stage. Details can be found elsewhere (Klingman, 1985).

Now that the appropriate descriptive equations have been established, it is sufficient for the model to provide the means by which the model parameters can be determined in an *a priori* manner. These are radial plug size distribution, length of the axial A/B cell, and individual linear velocities.

Alternating Flow Model Parameters

Radial variations in bed voidage or porosity are well documented experimentally (Ridgway and Tarbuck, 1968; Stanek and Eckert, 1979; Ouchiyama and Tanaka, 1984). Cohen and Metzner (1981) correlate the variations via a triregional model, which is given below for convenience:

Wall region ($x < 0.25$):

$$1 - \epsilon = 4.5(1 - \epsilon_{bulk})x(1 - 7x/9) \tag{25}$$

Transition region ($0.25 < x < 8$):

$$(\epsilon - \epsilon_{bulk})/(1 - \epsilon_{bulk}) = a_1 \exp(-a_1x) \cos(a_3x - a_4)\pi \tag{26}$$

Bulk region ($x < 8$):

$$\epsilon = \epsilon_{bulk} \tag{27}$$

where x is the distance, in pellet diameters, from the tube wall, ϵ is the local voidage and ϵ_{bulk} is not necessarily equal to the overall bed voidage, ϵ_b (Appendix). The constants are: $a_1 = 0.3463$, $a_2 = 0.4273$, $a_3 = 2.4509$, $a_4 = 2.2011$. These radial voidages are those averaged over the entire bed length.

Although the literature only hints at axial voidage variations (Schwartz and Smith, 1953; Bennett, 1972), they do exist. Figure 3a shows numerically determined axial void variations for $D_t/d_p = 3$, whereas Figure 3b shows experimentally measured voidages for $D_t/d_p = 6.6$. The numerical and experimental techniques are described elsewhere (Klingman, 1985). The peak-to-peak distance in the void fraction curves in Figure 3 indicates the void-full regions expected both radially and axially.

Radially, the distance can be found by determining the points

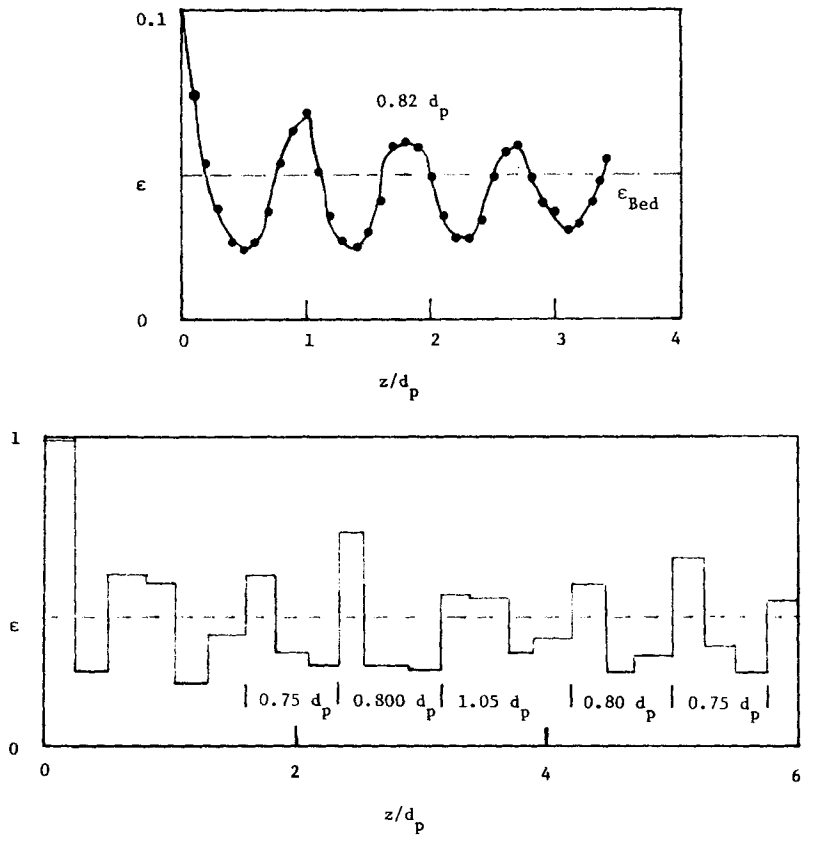

Figure 3. Axial voidage variations.
a. Numerical result for $D_t/d_p = 3.0$
b. Experimental result for $D_t/d_p = 5.04$

at which $\epsilon = \epsilon_b$, Eq. 26, and are given by

$$\cos(a_3x - a_4)\pi = 0$$

or

$$a_3x - a_4 = \ldots, -1.5, -0.5, 0.5, 1.5, \ldots \tag{28}$$

The values of x satisfying Eq. 28 are given in Table 1. The radial thickness of each void-full region would then be the distance between the ith and $(i + 2)$th zeros, since each zero indicates a transition from maximum to minimum voidage. Note from Table 1 that the distance between successive zeros is $0.408d_p$, yielding a radial void-full thickness of $0.816d_p$. (It may be of interest to also note that the center-to-center distance between spheres arranged in a hexagonal close-packed (HCP) pattern is $d_p(2/3)^{1/2} = 0.816d_p$.) Thus, the number of the radial void-full sections N_{rad} is given by

$$N_{rad} = (D_t/d_p)/0.816 \tag{29}$$

The actual value used in the model is N_{rad} rounded-up to the next even integer. The radius is divided into $(N_{rad}/2)$ equal increments, each of which is then subdivided to satisfy the radial distribution of void fraction. That is, for each of $(N_{rad}/2)$ increments, the voidage of any given A or B plug (void + full) must equal the radially averaged voidage given by Eq. 27 for that same interval:

$$2\int_{r_i}^{r_{i+2}} r\epsilon(r)\,dr = r_{hi}^2 - r_{lo}^2 \tag{30}$$

where the integration limits and notations are given in Figure 4. Note that the r's denote the normalized radial position, R/R_{tube}. The radii r_{hi} and r_{lo} are determined by the half-cell as shown in Figure 4. Also note that the A/B axial cell as a whole has two $(N_{rad}/2)$ number of void plugs. Therefore, $N = N_{rad}$.

Axially, the peak-to-peak distance can be found in an analogous manner. Figure 3 shows the cycle width, which represents the length of one half-cell, to be approximately $0.82d_p$, independent of D_t/d_p. Recall that the center-to-center distance for HCP spheres is $d_p(2/3)^{1/2} = 0.816d_p$; it is therefore assumed that this

Table 1. Half-Cycle Crossings of Radial Void Function

Righthand Side, Eq. 28	x Value
−1.5	0.286
−0.5	0.694
0.5	1.102
1.5	1.510
2.5	1.918
3.5	2.326
4.5	2.734

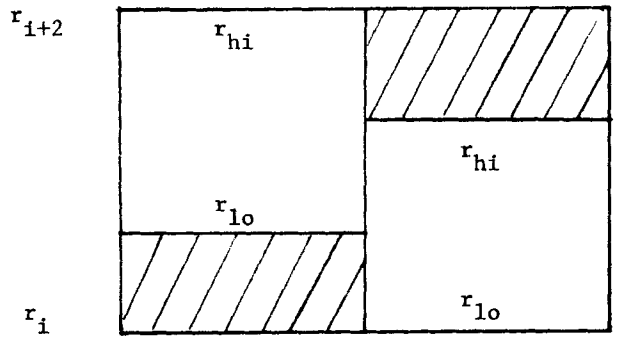

Figure 4. Intermediate radius integration limits.

is the axial voidage cycle width. Thus, the total (A/B) cell length is twice that amount. It follows then that the number of axially repeating (A/B) cells, N_{axial}, is given by

$$N_{axial} = Z_t/1.632d_p \tag{31}$$

where Z_t is the total tube length.

Consider now the individual linear velocities, U, in Eq. 10. Since the total flow rate Q_t was distributed to each void plug according to Eq. 4, it follows that $U_i = Q_i/A_i$ where A_i is the cross-sectional area of the void annulus for the ith radial void plug. These individual cross-sectional areas are determined from the radii defined by Eq. 30. These linear velocities are scaled by dividing by the average interstitial bed velocity, $U_b = Q_t/(\epsilon_b A_t)$, or

$$U_i/U_b = \epsilon_b \left(\frac{Q_i}{Q_t}\right) \Big/ \left(\frac{A_i}{A_t}\right) \tag{32}$$

The delay times in each annulus are given by the half-cell plug length divided by the corresponding velocity and are scaled by dividing by the average bed holdup time, $\tau = Z_t/U_b$, to give

$$\tau_i/\tau = \left(\frac{A_i}{A_t}\right) \Big/ (2N_{axial}\epsilon_b Q_i/Q_t) \tag{33}$$

since there are $(2N_{axial})$ half-cells (plug lengths) across the total bed length Z_t.

Comparisons were made between the radial velocity profiles predicted by Eq. 32 and those reported in the literature (Schwartz and Smith, 1953; Schertz and Bischoff, 1969; Marivoet et al., 1974). In all cases compared (Klingman, 1985), the alternating flow model predictions followed the data well except at the wall and the center. The AFM predictions, when compared with those by Schwartz and Smith (1953) and Schertz and Bischoff (1969), yielded a larger change near the wall and a smaller velocity at the center, consistent with the findings of Vortmeyer and Schuster (1983). A comparison with the detailed data reported by Marivoet et al. (1974) is shown in Figure 5.

An examination of the relationships derived so far for determining AFM parameters reveals one key point: only geometric factors $(D_t/d_p, Z_t/d_p, \epsilon_b)$ are required to predict the mass dispersion in packed beds. Thus, the alternating flow model is predictive; its parameters are determined *a priori* with no need to back-fit them to dispersion data. These parameters are the size

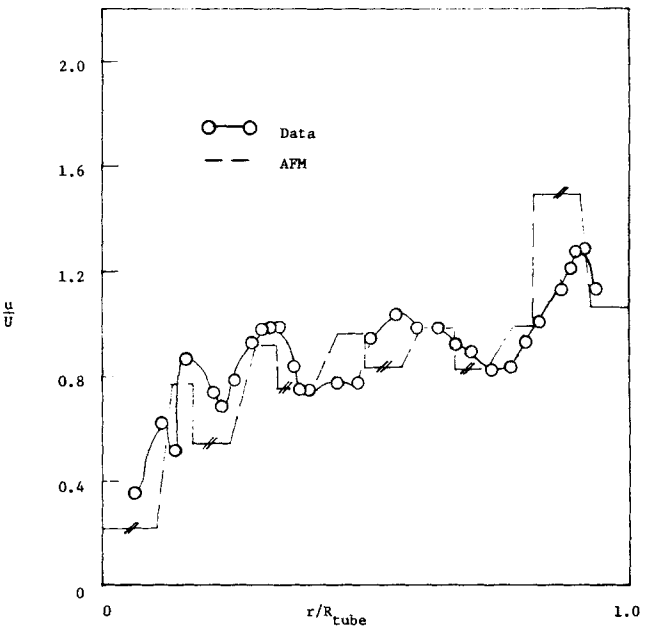

Figure 5. Radial velocity profile.
$D_t/d_p = 9.4$, data of Marivoet et al. (1974).

of axial cell length, the distribution of radial plugs, and the distribution of flows for the steady state dispersion; the velocity distribution is required in addition for the transient dispersion. The results obtained so far for the AFM can now be used to make comparisons with the literature dispersion data. Complete AFM equations are summarized in the Appendix.

Comparisons with Experimental Dispersion Data

Attempts were made to make comparisons with the literature data in the widest possible ranges of geometric factors. The ranges for the comparisons in Figure 6 for steady state radial concentration profiles at fixed positions are: $5.6 < D_t/d_p < 54$, $100 < Re_p < 1{,}000$, and $10 < Z_t/d_p < 100$. Figure 7 shows axial profiles at two fixed radial positions for $D_t/d_p = 12.8$. Figure 8 gives two F-curves: one for $D_t/d_p = 15.9$ and $Z_t/d_p = 191$, and another for $D_t/d_p = 8$ and $Z_t/d_p = 32$. Both gases and liquids are represented, as the details on the experimental conditions summarized in Table 2 reveal. The experimental results are compared to the prediction via:

1. Fickian predictive: dispersion coefficients obtained via correlations available in the literature (Wen and Fan, 1975; Levenspiel, 1962)
   (a) steady state via Eq. 15 of Gunn and Pryce (1969)
   (b) transient via Eq. 19 of Danckwerts (1953)
2. Alternating flow model predictions

These figures do not show the profiles obtained by back-fitting dispersion coefficients to the data since, at any given axial position it is possible to obtain a nearly perfect fit. However, the parameters chosen to fit the data at an axial position do not fit well the data at other positions.

In the steady state cases, Figures 6 and 7, the vertical axis represents point-value concentrations scaled by the average measured effluent concentration, C_a, which can be calculated at any given axial position as C_a = (total amount of tracer material)/(total amount of fluid). Solutions of the Fickian analogy,

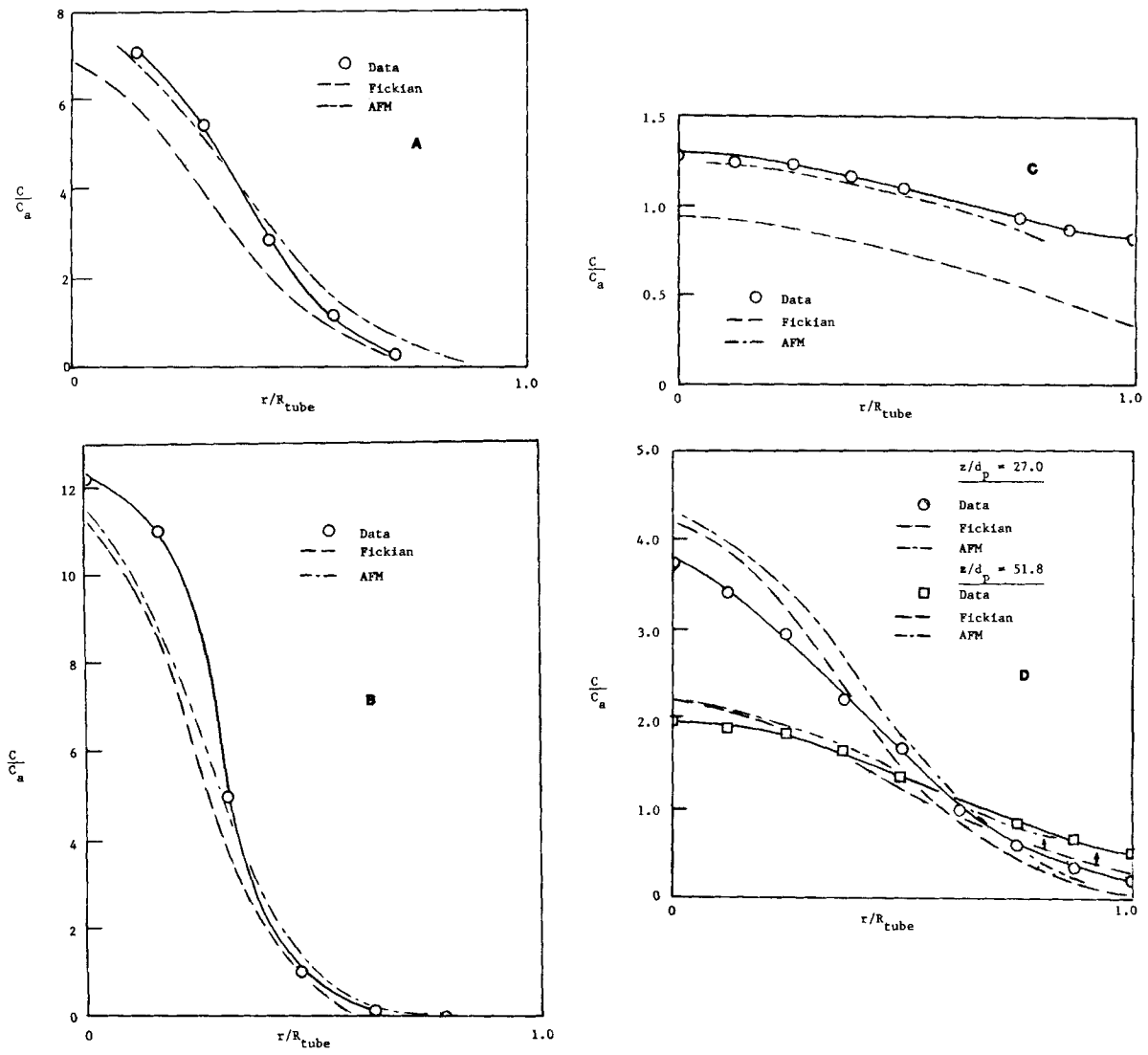

Figure 6. Steady state radial concentration profiles.

A. $D_t/d_p = 15$, $Z/d_p = 23$, data of Gunn and Pryce (1969)
B. $D_t/d_p = 54.3$, $Z/d_p = 180$, data of Latinen (1954)
C. $D_t/d_p = 5.6$, $Z/d_p = 23$, data of Fahien and Smith (1955)
D. $D_t/d_p = 12.8$, $Z/d_p = 27$ and 52, data of Fahien and Smith (1955)

Eq. 1, for C/C_a as a function of radial and axial position are given elsewhere (Gunn and Pryce, 1969; Danckwerts, 1953; Cairns and Prausnitz, 1960; Wen and Fan, 1975). For the AFM, the scaled concentrations become:

$$C_i/C_a = C_iQ_i/\Sigma C_iQ_i \tag{34}$$

with $i = 2, 4, 6, \ldots, N$ for the A half-cell, and $i = 1, 3, 5, \ldots, N-1$ for the B half-cell. The subscript i implies that the concentration in that given annular plug is constant. To alleviate discrete (stepwise) concentration profiles, the figure captions give the values calculated from Eq. 34 at each plug's midpoint radius.

Figure 6 indicates good agreement of the AFM with experiment over a wide range of D_t/d_p. However, Figures 6d and 7, which show axial variations for $D_t/d_p = 12.8$, indicate that at low Z_t/d_p neither the AFM nor the Fickian analogy closely follows the observed dispersion behavior. However, the agreement is quite good for $Z_t/d_p > 25.6$ (or about two tube diameters). This behavior is also borne out in Table 3, which compares AFM and Fickian predictions to observed values of centerline concentrations for $5.6 < D_t/d_p < 25.6$ as given by Fahien and Smith (1955). Note the improvement in both models as Z_t/D_t increases. This can probably be attributed to entrance effects since the tracer injection tube creates a disturbance in the flow pattern and in the packing pattern that may each take some distance to settle out. For example, in empty tubes the flow disturbance created by a barrier requires several pipe diameters to settle out (Daugherty and Franzini, 1977) as compared to an apparent settling length here of about two pipe diameters.

In all steady state cases, the AFM results equal or surpass the Fickian predictions. These results lend support to the methods for sizing plugs, Eq. 30, for determining axial cell length, and for distributing the flows, Eqs. 4, 6, and 8.

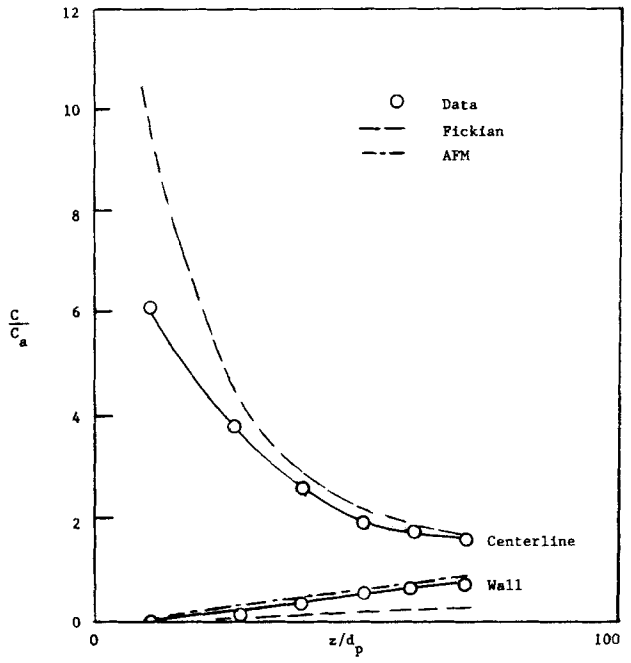

Figure 7. Steady state axial concentration profiles.
D_t/d_p = 12.8, data of Fahien and Smith (1955)

Transient (*F*-curve) AFM and Fickian predictions using the dispersion coefficients from two different sources (Levenspiel, 1962; Wen and Fan, 1975) are compared to data in Figure 8; see Table 2 for the system description. These figures indicate that the AFM again surpasses the Fickian analogy.

The lag of the AFM behind the data may be due to using an incorrect ϵ_b to determine the velocity profile, Eq. 32. The ϵ_b values used in the AFM simulations for Figure 8 were based on the ϵ_b vs. D_t/d_p correlation given by Leva and Grummer (1974a, b) since neither researcher gave explicit bed porosity values. If ϵ_b is actually larger than the selected values, then the scaled velocities would be proportionately faster (see Eq. 32) and the entire AFM *F*-curve would shift left in time. The shift should become less pronounced as the number of mixes increases since increasing the exponent (the axial cell number, n) or dimension (D_t/d_p or N_{rad}) of Eq. 11 tends to damp any discontinuities in the velocity profile.

Alternating Flow Model for Heat Dispersion

While the same dispersion pattern as in mass dispersion is valid for the heat dispersion in a packed bed, the packing and wall can no longer be considered inert since heat transfers in from the wall and disperses radially from the bulk fluid to the packing. This nature of heat dispersion is in fact the reason why it is so much more difficult to describe the heat dispersion than the mass dispersion.

In the context of the AFM, equations describing the solid plugs must also be considered. Note from Figure 2 that since the radial void-full pattern depends on the half-cell, several types of plugs must be considered:

1. Main fluid plug—an annulus surrounded by different packing annuli (e.g., plugs *A*2, *A*4, *B*3, and *B*5 of Figure 2)
2. Main solid plugs—an annulus surrounded by different fluid annuli (e.g., solid plugs surrounded by *A*3, *A*5, *B*2, *B*3, and *B*4 of Figure 2)
3. Center solid plug—completely surrounded by same fluid plug (i.e., plug *A*1 of Figure 2)
4. Center fluid plug—completely surrounded by same solid plug (i.e., plug *B*1 of Figure 2)
5. Wall fluid plug—tube wall on one side and solid plug on the other (e.g., plug *A*6 of Figure 2)
6. Wall solid plug—tube wall on one side and fluid plug on the other (e.g., solid plug above *B*5 of Figure 2)

The AFM assumes that no heat transfers via radiation, that no heat conducts between solid plugs, that heat convects from wall to fluid across a wall film resistance (h_w) and from wall to solid via conduction, and that heat convects from fluid to packing (solid plugs) across a pellet film resistance (h_p). These assumptions, together with the underlying assumptions of plug flow through each of the void radial plugs and the mixing at plug outlets via the matrix mixing equations for mass dispersion, will be used to develop appropriate heat dispersion relationships for each type of plug.

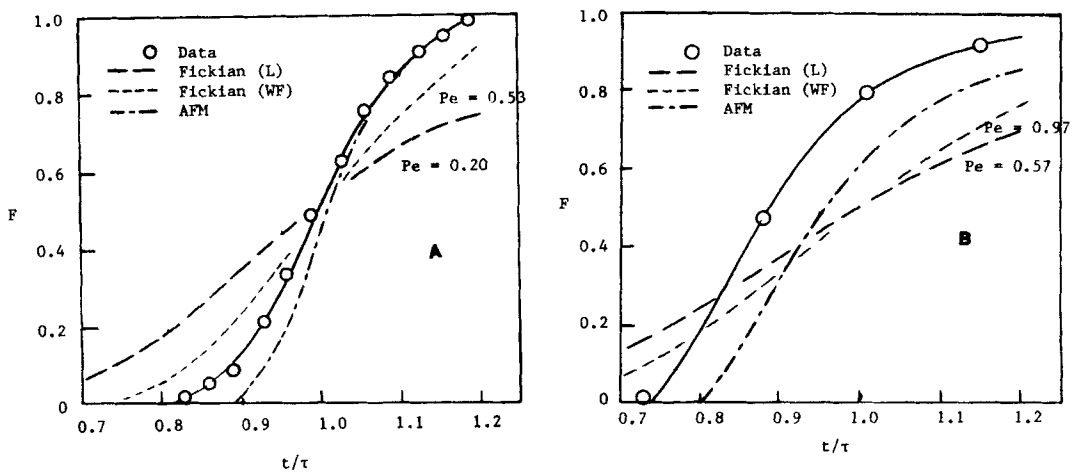

Figure 8. *F*-curves: *L* based on correlation by Levenspiel (1962), *WF* based on correlation by Wen and Fan (1975).
a. D_t/d_p = 15.9, Z/d_p = 191, data of Cairns and Prausnitz (1969).
b. D_t/d_p = 8.0, Z/d_p = 32, data of Jacques and Vermeulen (1957)

Table 2. Data Used for Comparison of Concentrations

Source	Type*	D_t cm	d_p cm	Tracer/ Bulk	Re_p	Z/d_p
Fahien & Smith (1955)	SS	5.08	0.4	CO_2/air	150	10–70
		−10.16	−0.91		−900	
Gunn & Pryce (1969)	SS	8.89	0.6	Ar/air	121	23
Latinen (1954)	SS	5.08	0.094	Dye/water	102	180
Cairns & Prausnitz (1960)	Trans	5.08	0.32	NaOh/water	128	191
Jacques & Vermeulen (1957)	Trans	15.24	1.91	NaOH/water	130**	32

*SS, steady state; Trans, transient

**Data read directly from Jacques and Vermeulen Figure 32, which was assumed to represent run 217-2 (2 gpm), not run 217-1 as stated. If this assumption is not made, the data imply that the F-curve reaches 50% only after two vessel holdup times, a situation that seems highly unlikely.

Main fluid plug

Consider a heat balance on a fluid element as shown in Figure 9a. The element gains heat due to bulk inflow and from the warmer solid above, and loses heat with the bulk outflow and to the cooler solid below. Thus,

$$\rho C_p Q_j \frac{dT_j}{dz} = h_p a_{j,j+1}(t_{j+1} - T_j) - h_p a_{j,j-1}(T_j - t_{j-1}) \quad (35)$$

where t is the solid temperature, T is the fluid temperature, Q_j is the fluid volumetric flow rate through the jth plug, and z refers to the distance from the plug entrance, Figure 9a. Note that the mass flux G is related to AFM parameters via

$$G = \rho \sum_j Q_j / A_t \quad (36)$$

where A_t is the tube cross-sectional area.

The heat transfer areas $a_{j,j+1}$ and $a_{j,j-1}$ are the areas per unit length available for heat transfer from upper solid to fluid and from fluid to lower solid, respectively, which are based on the total surface area available within a solid plug. If it is assumed that half of this area faces up and half down, one has

$$a_{j,j+1} = \tfrac{1}{2}\pi R_t^2 (r_{j+1}^2 - r_j^2)(S_p/V_p)$$
$$a_{j,j-1} = \tfrac{1}{2}\pi R_t^2 (r_{j-1}^2 - r_{j-2}^2)(S_p/V_p) \quad (37)$$

where R_t is the tube radius and r_j's were defined earlier. Note that the effect of pellet shape on these areas is implied by the term S_p/V_p, which is the ratio of external surface area to volume. For spherical pellets it is $6/d_p$; it is $4/d_p$ for cylinders.

Table 3. Centerline Concentrations

			Centerline Concentration*		
D_t/d_p	Z_t/d_p	Z_t/D_t	Data	AFM	Fickian
25.6	52.0	2.0	4.8	8.6	8.7
13.3	27.1	2.0	2.8	4.2	4.5
11.1	22.6	2.0	2.3	4.0	3.7
6.9	14.0	2.0	1.3	2.2	2.3
19.2	52.0	3.0	3.8	4.8	4.9
8.3	22.6	3.0	1.8	2.0	2.1
12.8	52.0	4.0	2.2	2.1	2.2
5.6	22.6	4.0	1.3	1.3	0.95

*All data from Fahien and Smith (1955).

Equations for other types of plug are summarized in Table 4. Details for the relationships are given elsewhere (Klingman, 1985).

Condensation of equations and solution procedures

The description of the complete radial profile at any given z within an A half-cell requires Eqs. 39 and 40 for t_j (j = 1, 3, 5, . . . , N − 1) and Eqs. 35 and 42 for T_j (j = 2, 4, . . . , N), Figure 9. Equations 39 and 43 for t_j (j = 2, 4, 6, . . . , N) and Eqs. 35 and 41 for T_j (j = 1, 3, 5, . . . , N − 1) are required for a B half-cell. Table 4 presents Eqs. 38–42. Since the temperatures vary with z, these equation sets must be integrated from plug inlet to outlet before mixing calculations can be made. After the cells and plugs are sized according to D_t/d_p and ϵ_{bed} and the flows subdivided and mixing matrices determined, the temperature profile at any given axial position can be obtained in the following manner:

1. Set all inlet temperatures (solid and fluid) to T_{in}.
2. Within the A half-cell, integrate Eqs. 35 and 42 for j = 2, 4, . . . , N − 2 from z = 0 to $z = 0.816 d_p$ (the length of one half-

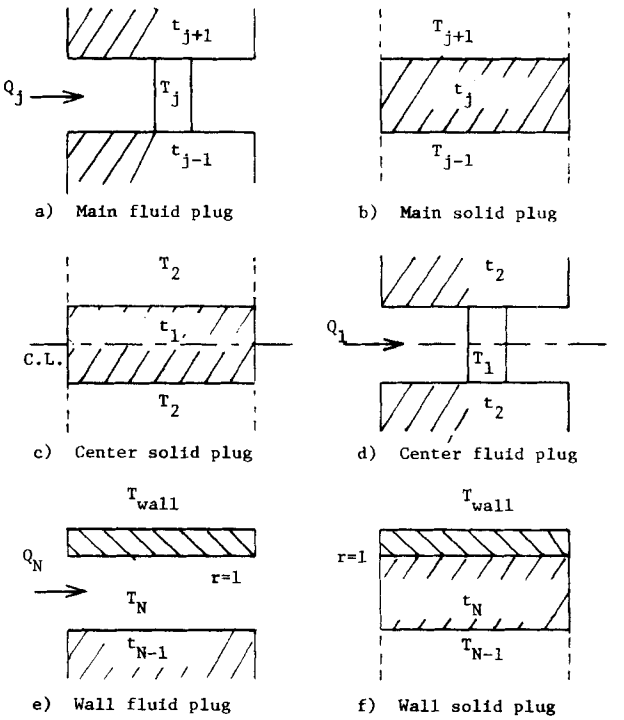

Figure 9. Plug types for AFM heat dispersion analysis.

Table 4. Equations for Various Plug Types in Figure 9

Plug Type	Balance Equation	Eq. No.
Main fluid plug	$\rho C_p Q_j \frac{dT_j}{dz} = h_p a_{j,j+1}(t_{j+1} - T_j) - h_p a_{j,j-1}(T_j - t_{j-1})$	(38)
Main solid plug	$t_j(z) = 0.5[T_{j+1}(z) + T_{j-1}(z)]$	(39)
Center solid plug	$t_1(z) = T_2(z)$	(40)
Center fluid plug	$\rho C_p Q_1 \frac{dT_1}{dz} = h_p a_{1,2}[t_2(z) - T_1(z)]$	(41)
Wall fluid plug	$\rho C_p Q_N \frac{dT_N}{dz} = h_w 2\pi R_t (T_w - T_N)$	(42)
Wall solid plug	$t_N(z) = 0.1\ T_w + 0.9 T_{N-1}$	(43)

cell). Note that this must be done numerically as the interdependence of the equations precludes analytical results. At each integration step, obtain new solid temperatures via Eqs. 39 and 40 for $j = 1, 3, 5, \ldots, N-1$. The outlet fluid temperatures (T_2, T_4, ..., T_N) become the elements of the $(N/2)$-long vector $\boldsymbol{T}_{Aout,N}$, where N is the current cell number.

3. Calculate the next B half-cell inlet temperatures via the previously defined mixing matrix, $\boldsymbol{R}$, used in the mass dispersion calculations:

$$\boldsymbol{T}_{Bin,n} = \boldsymbol{R}\boldsymbol{T}_{Aout,n} \tag{44}$$

where $\boldsymbol{T}_{Bin} = (T_1, T_3, \ldots, T_{N-1})$

4. Integrate Eqs. 35 and 43 for $j = 3, 5, \ldots, N-1$ from B half-cell inlet to outlet, calculating new solid temperatures at each integration step (Eqs. 11 and 19 for $j = 2, 4, \ldots, N$). The outlet fluid temperatures (T_1, T_3, ..., T_{N-1}) become the elements of the $(N/2)$-long vector $\boldsymbol{T}_{Bout,N}$.

5. Calculate next A half-cell inlet temperatures via the previously defined mixing matrix $\boldsymbol{S}$ used in the mass dispersion calculations:

$$\boldsymbol{T}_{Ain,n+1} = \boldsymbol{S}\boldsymbol{T}_{Bout,n} \tag{45}$$

6. Repeat steps 2 to 5 until the desired number of axial cells has been traversed.

AFM Model Parameters h_p and h_w

Of the parameters necessary for heat but not mass dispersion, $a_{j,j+1}$ are defined by the AFM in terms of packing geometry, Eq. 37. The nature of the coefficients h_p and h_w on the other hand prevents them from being determined solely by geometry. In fact, previous studies of flow around submerged objects (Bird et al., 1960) and in empty tubes (McCabe and Smith, 1976) show that film coefficients must be correlated to system variables such as pellet or tube size, total flow rate, friction factor, and fluid properties (e.g., thermal conductivity and specific heat). The AFM thus draws on this experience to obtain general correlation forms for h_p and h_w.

Pellet film coefficient, h_p

Forced-convection heat transfer from a single sphere in an infinite fluid moving at velocity v^* according to Ranz and Marshall (1952), has been related in the following manner, by Bird et al. (1960, p. 409):

$$\frac{h_p d_p}{\lambda} = 2.0 + \left(\frac{C_p \mu}{\lambda}\right)^{1/3} \left(\frac{d_p G}{\mu}\right)^{1/2} \tag{46}$$

where λ is the fluid thermal conductivity, the mass flux $G = \rho v^*$, C_p is the fluid specific heat, and ρ is the fluid density. For a fluid with constant physical properties, Eq. 46 can be written as

$$h_p = k_a + K' \left(\frac{G}{d_p}\right)^{1/2}; \quad G = G_{int} \tag{47}$$

where k_a and K' are constants. At high flow rates, the second term on the righthand side of Eq. 46 dominates, yielding

$$h_p = K' \left(\frac{G}{d_p}\right)^{1/2}; \quad G = G_{int} \tag{48}$$

Bird et al. (1960, p. 408) also give a graphical correlation (from Sherwood and Pigford, 1952, p. 70) of h_p for long cylinders, which can be represented in the same form as Eq. 48 (Klingman, 1985).

According to these relationships, then, h_p should vary as $(G_{int}/d_p)^{1/2}$ whether or not the pellets are spherical or cylindrical.

Wall heat transfer coefficient, h_w

Forced-convection heat transfer in empty tubes has been related in many forms to system parameters (Bennett and Myers, 1982; Greenkorn and Kessler, 1972; McCabe and Smith, 1976). McCabe and Smith, for example, give a collection of these correlations for smooth and rough pipes. Of these, the AFM uses the following equation as a guide for a general form of correlation between h_w and other system parameters:

$$\frac{h_w}{C_p G} = \frac{f}{\psi(f)} \tag{49}$$

where f is the friction factor and $\psi(f)$ is some function of f.

The relationship of f vs. Re and relative roughness, δ/D_t, in pipes is well established (Greenkorn and Kessler, 1972). Each (δ/D_t) establishes a separate curve (with f decreasing as Re increases), which can be represented by several segments over

which

$$f = k_f / Re^n \tag{50}$$

where K_f is a constant. For smooth pipes n is essentially constant, whereas for rough pipes n is maximum at low Re and equal to zero at complete turbulence. Since trends in h_w are desired, Eq. 50 can be combined with Eq. 49 to give [if $\psi(f) = 1$]

$$h_w = K_f C_p G_{int} Re^{-n} \tag{51}$$

Hence, for a fluid with constant physical properties

$$h_w = K_w \frac{G_{int}^{1-n}}{D_t^n} = K_w \frac{G_{int}^m}{D_t^{1-m}} \tag{52}$$

Other parameters influenced by pellet shape

To solve the AFM equations, the cells and plugs must be sized according to D_t, d_p, and ϵ_{bed} so that the flow rates and mixing matrices can be determined. The mass dispersion established these parameters for spherical packing, where radial and axial porosity profiles showed oscillations about ϵ_{bed} with cycle widths of $0.816 d_p$. But, one may question whether similar patterns would hold with cylindrical pellets.

Roblee et al. (1958) report radial porosity profiles for beds packed with cylinders. The profiles indeed show oscillation about the lower ϵ_{bed}. However, no definite conclusions regarding the actual cycle width can be drawn from their work since they present segments, or disks, one pellet diameter long. Because of the expected axial oscillations in porosity, one pellet diameter is too short to represent average bed values and too long to yield axial cycle widths. Indeed, the data show two distinct profiles, each with a different period of oscillation.

Consider the orientation of cylindrical pellets of diameter d and length ℓ as they are packed into a tube. If it is assumed that the perpendicular (pellet axis at a right angle to flow direction) and parallel (pellet axis parallel to flow direction) orientations are equally probable, then the fluid can encounter a barrier of width d or ℓ with equal probability. Thus, the AFM uses the geometric mean

$$d_p = [(d^2 + \ell^2)/2]^{1/2} \tag{53}$$

as the effective pellet diameter. Calculating d_p in this way assures that if $d = \ell$, $d_p = d$, whereas the equivalent volume argument leads to

$$d_p = d(1.5)^{1/3} \tag{54}$$

regardless of the aspect ratio d/ℓ. The relationships presented for spherical pellets then use the d_p of Eq. 53 (and the corresponding D_t/d_p) together with the lower ϵ_{bed} to determine axial cell length and radial plug width as presented for the mass dispersion case. The individual flows and weighting matrices follow accordingly.

Determination of film coefficients

The previous section established that h_p should be proportional to the square root of (G_{int}/d_p), Eq. 48, with h_p for cylindrical pellets exceeding h_p for spherical pellets under equal conditions. This in turn implies that if h_p is known at one G_{int}/d_p or base case for a given packing (e.g., smooth spheres, rough spheres, smooth cylinders, etc.), the h_p at any other G_{int}/d_p can be determined from

$$h_p = h_{p,base} \left(\frac{G_{int}}{G_{int,base}} \cdot \frac{d_{p,base}}{d_p} \right)^{1/2} \tag{55}$$

where $G_{int} = \rho Q / A_{tube} \epsilon_{bed}$.

It was also established that h_w should vary as G_{int}^m where m depends on system variables such as tube diameter, pipe material, and degree of turbulence (i.e., range of G). Since turbulence in packed beds cannot readily be defined, the value of m cannot be specified *a priori* but must be fitted to data for a given set of system variables (D_t, pipe material) over the desired range of flow rates. While this may at first seem dissatisfying, note that since h_p is predetermined according to a base case, h_w remains the sole parameter to be correlated.

If the tube is hydraulically smooth (e.g., glass or brass), m in Eq. 52 should be constant over a wide range of Re (flow rates) (Greenkorn and Kessler, 1972). Curve-fitting the empty tube value of f at Re = 60,000 and 250,000 leads to $4f = 0.184 R_e^{-0.202}$. Thus, $n = 0.2$ and $m = 0.8$, Eq. 52, so that

$$h_w = h_{w,base} (G_{int}/G_{int,base})^{0.8} \tag{56}$$

should hold for smooth tubes. Stretching the analogy further would imply that experiments carried out in rough tubes should lead to $m > 0.8$.

The hypothesis that pellet shape would affect the magnitude but not the functional form of h_p can be tested by letting

$$h_p = \gamma h_{p,sphere} = \gamma h_{p,base} \left(\frac{G_{int}}{G_{int,base}} \cdot \frac{d_p}{d_{p,base}} \right)^{1/2} \tag{57}$$

where γ is a constant that accounts for enhanced heat transfer due to increased turbulence from nonsmooth or asymmetric pellets. For cylindrical pellets, then, a new base case must be selected and the coefficients h_p and h_w again fitted by trial and error. The constant γ can then be back-calculated from Eq. 57. For the hypothesis to be valid, γ should exceed 1 but should remain constant for all systems employing cylindrical pellets.

Comparison with Experimental Data

Comparisons are limited to the literature data that contain measurements of the outlet temperature and radial and/or axial temperature profiles, or centerline temperature, which are needed to establish the base cases for the correlations for h_p and h_w.

Yagi and Wakao (1959) give both centerline and bulk-average outlet temperatures for their experiments in a (smooth) brass tube packed with smooth, uniformly sized glass pellets. They used one tube size with two different pellet sizes over a range of particle Reynolds number, $100 < Re_p < 700$. For their run F-1 (G = 2,740 kg/h · m^2, D_t = 3.6 cm, d_p = 0.6 cm), they also give the axial variation in centerline temperature. This was therefore selected as the base case.

Figure 10 compares AFM results (h_p = 0.002 cal/s · cm^2 · K,

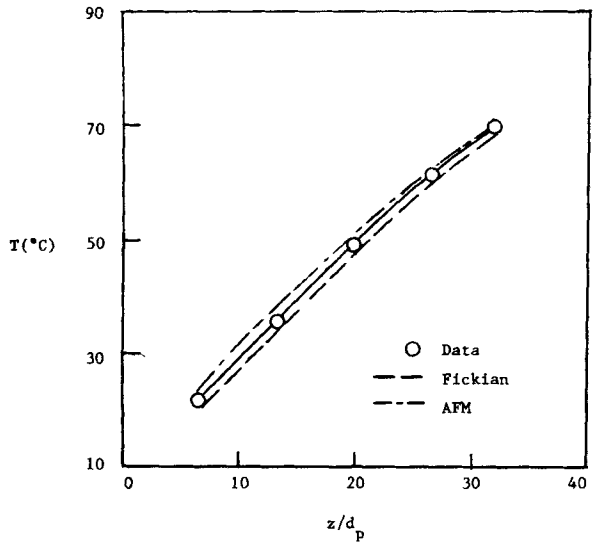

Figure 10. Axial temperature profile.
$Re_p = 234$, $D_t/d_p = 6$, data of Yagi and Wakao (1959)

$h_{w,base} = 0.002$ cal/s · cm^2 · K) and best-fit Fickian profile and $T_{b,out}$ to the data for the base case.

Table 5 compares AFM and best-fit Fickian results to outlet centerline and bulk-average temperature data for all other E ($d_p = 0.26$ cm) and F ($d_p = 0.6$) runs of Yagi and Wakao with h_p determined from Eq. 55 and h_w from Eq. 56, i.e., Eq. 52 with $m = 0.8$. In predicting bulk outlet values, the AFM surpasses the Fickian analogy in all but three of the cases (in two of these it differs from the Fickian back-fit by only 0.2°C). In predicting outlet centerline temperatures the AFM again surpasses the Fickian back-fit in all but three cases (in two of these the AFM prediction of the corresponding $T_{b,out}$ is within 0.2°C of the Fickian back-fit). The worst AFM fit is for the centerline temperature of the $Re_p = 106$ case. But, recall from earlier discussion that the relationship given by Eq. 55 is a simplified version of

Table 5. AFM for Heat Dispersion in Smooth Brass Tube Packed with Glass Spheres

d_p cm	Re_p	Item, at exit	Data	AFM*	Fickian**
0.6	234	t_c	69.8	69.9	68.5
		T_b	78.8	78.1	77.9
0.6	382	t_c	63.6	62.3	77.9
		T_b	74.8	71.7	73.8
0.6	691	t_c	56.1	57.8	54.1
		T_b	69.2	67.9	67.7
0.26	106†	t_c	65.3	60.2	64.0
		T_b	77.3	77.8	76.4
0.26	183	t_c	51.3	49.4	50.1
		T_b	69.7	70.4	69.0
0.26	238	t_c	52.1	48.8	49.7
		T_b	68.1	69.9	66.5
0.26	323	t_c	50.1	48.2	47.9
		T_b	67.1	69.3	65.5

*AFM predictive, used $\epsilon_{bed} \sim 0.40$ in all calculations
**Fickian back-fit; parameters specified by Klingman (1985)
†AFM, used laminar/transition hydraulic resistances to radially distributed flows
All data from Yagi and Wakao (1959); air at inlet $T_{in} = 20$°C; $t_{wall} = 100$°C; $D_t = 3.6$ cm in all cases.

Eq. 47. If the flow rate or Re_p is low, the constant term may begin to assert itself, i.e., the h_p based on the complete version, Eq. 47, would be larger than h_p determined from the simpler version, Eq. 54. Because only one heat dispersion data set was available at $Re_p < 150$, the h_p values were not fitted to the complete form, Eq. 47.

According to these arguments, then, the use of Eq. 55 to determine h_p is justified. And the fact that $m = 0.8$ for h_w correlates the data so well justifies not only the form of h_w given by Eq. 52 but also the friction factor analogy. Note that $m = 0.8$ was predicted solely from relating heat to friction factors in empty tubes, Eq. 56.

While $T_{b,out}$ provides sufficient information with which to correlate h_w as discussed in the previous section, the absence of radial and axial temperature profiles would prevent double-checking the goodness of fit. But, the form of Eq. 52 implies that a log-log plot of h_w vs. G should provide a straight line of slope m. A distinct change in slope at high or low G would indicate that the system has moved from one f vs. Re regime to another.

Such log-log plots of AFM h_w vs. flow rate for smooth glass spherical packing in standard pipe (Leva, 1947) are shown in Figure 11a for the smaller tube ($D_t = 1.58$ cm, $D_t/d_p = 4.95$, runs 100a–e) and in Figure 11b for the larger tube ($D_t = 5.26$ cm, $D_t/d_p = 5.33$, runs 9a–h). Each plot shows a definite straight line segment with the expected change in slope (m not constant for all G in rough tubes) and with essentially no scatter in the constant slope segment. The values of $m = 1.0$ for the smaller tube and $m = 0.89$ for the larger tube are consistent with the friction factor analogy discussed earlier: for tubes of the same material, m should be inversely proportional to D_t.

The available literature data for cylindrical pellets provide only radial temperature profiles (albeit at several bed depths by Coberly and Marshall, 1951) without corresponding $T_{b,out}$ values. Fitting h_w to data of this type presents some difficulty as the distance between temperature measurement point and bed exit increases. Unless the temperatures are actually measured inside the packed section, the difficulty in fitting h_w would also increase as the bed length decreases.

Coberly and Marshall (1951) ran their experiments with the thermowells nearly touching the packing. They also measured radial profiles at several bed depths, keeping all other system variables constant. Thus, if h_w and h_p are fitted to their data at maximum bed depth, the corresponding AFM-predicted axial-radial temperature profiles can be compared to data to provide added insight into the goodness of fit. These researchers studied several system geometries, but the system of 0.95 cm × 1.27 cm cylinders packed in a 12.7 cm tube was selected for AFM comparison since it provided the smallest D_t/d_p. The geometric mean d_p, Eq. 53, for cylinders of this aspect ratio is 1.12 cm, so that $D_t/d_p = 11.3$.

Figure 12 shows the log-log plot of AFM h_w vs. flow rate for this system, and Figure 13 compares the corresponding AFM axial temperature profiles at two radial positions to experimental data. In Figure 12, note the constant slope segment breaking off at low flow rates, in accordance with the friction factor analogy. The high value of $m = 2$ cannot, however, be explained within that framework. Note from Figure 13 how closely AFM results follow the axial temperature profiles. The largest deviations are at small r near $z = 0$. But, as indicated in the figure, the flow rates at these inner radii are small proportions of the total stream. Thus, those points with the largest absolute error in tem-

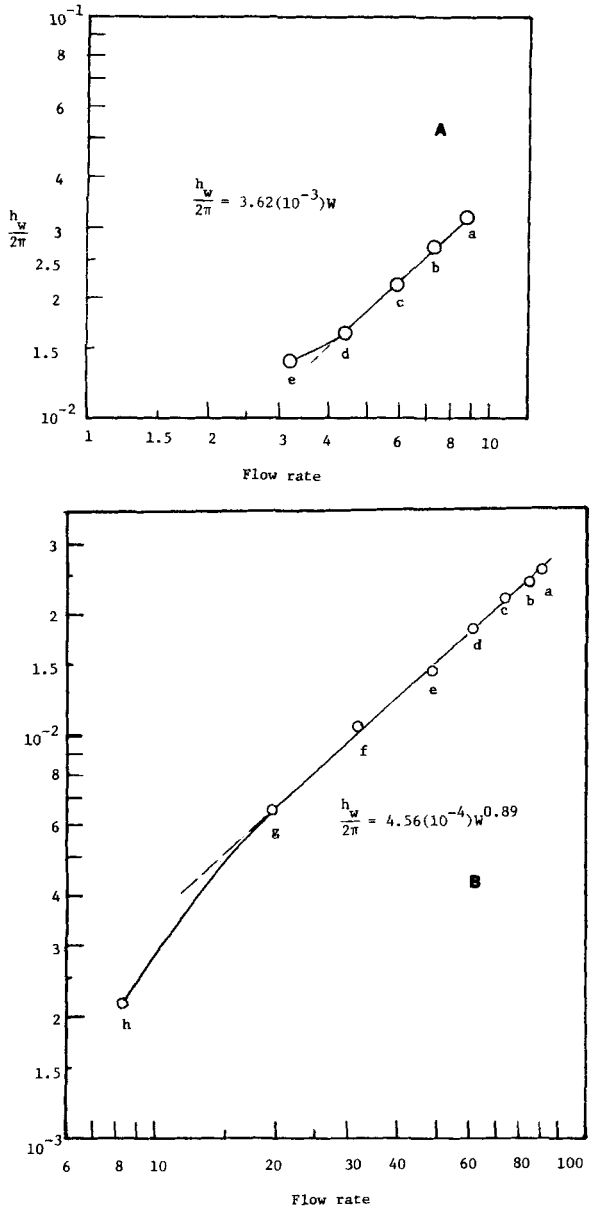

Figure 11. AFM wall film heat transfer coefficients, data of Leva (1947).

a. Runs 100a–e, $D_t/d_p \approx 4.95$, $D_t = 1.6$ cm
b. Runs 9a–h, $D_t/d_p = 5.3$, $D_t = 5.3$ cm

perature will have the smallest relative contribution to the overall system.

The constant γ, used to determine h_p via Eq. 57, was determined from run 1–6 to be 1.33. This value of $\gamma > 1$ is consistent with the idea that cylindrical pellet increase turbulence and enhance heat transfer over what would be expected for spherical pellets.

Figure 14 shows the log-log plot of AFM h_w vs. flow rate for the data of Lerou and Froment (1977) ($D_t = 9.9$ cm, cylindrical pellets with $d = \ell = d_p = 0.95$ cm, bed length = 48.8 cm). This plot also shows consistency with the friction factor analogy as the constant slope of $m = 0.66$ at low flow rate. The magnitude of $m < 0.8$ cannot, however, be explained within the framework of the friction factor analogy. Since neither $T_{b,out}$ values nor

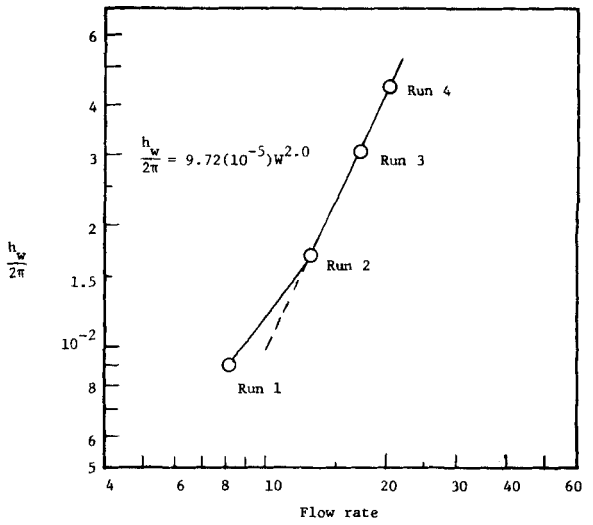

Figure 12. AFM wall film coefficient.

Data of Coberly and Marshall (1951) for 0.95 cm × 1.27 cm cylindrical pellets

axial temperature profiles are available for these experiments, no further checking via data can be done.

Summary

The alternating flow model is a viable alternative to the traditional Fickian analogy approach for modeling dispersion in packed beds. Not only does the AFM require fewer correlated parameters than the Fickian analogy, it also meets all the dis-

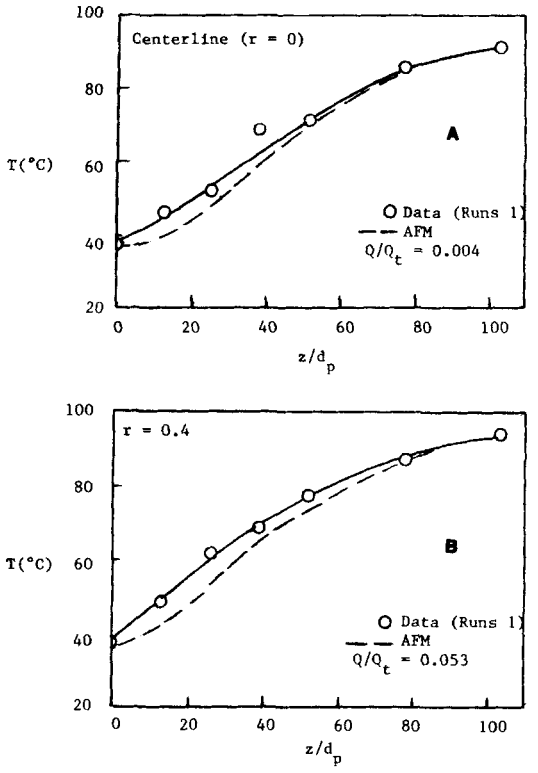

Figure 13. Axial temperature profiles.

Data of Coberly and Marshall (1951) for 0.95 cm × 1.27 cm cylindrical pellets at two radial positions

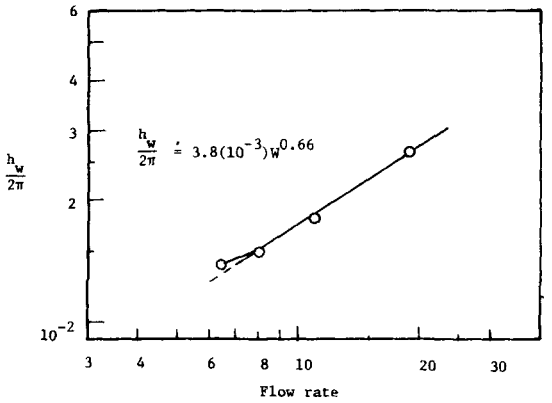

Figure 14. AFM wall film coefficient.
Data of Lerou and Froment (1977)

persion model acceptability criteria set forth in the Introduction. The AFM can also predict, solely from system geometry, the observed velocity profile trends for a packed bed.

For mass dispersion, the AFM is totally predictive: all model parameters are determined *a priori* from bed voidage and relative size of tube to pellet. The AFM equalled or surpassed the Fickian analogy in following the experimental data of the simple mass dispersion cases considered.

For heat dispersion, the AFM requires back-fitting one parameter, the wall film coefficient h_w, to each new system for the base case. The complexity of turbulent heat convection explains this need for back-fitting h_w. A friction factor analogy sheds light on the observed h_w vs. G^m relationship and can even predict the exponent, m, for smooth tubes. Most of the heat dispersion cases considered show the AFM to follow experimental data at least as closely as the back-fit Fickian analogy.

Finally, the limitations of the model have to be recognized. Clearly, the ordered flow implied in the model indicates that it is not satisfactory for very low bulk velocity of flow rate. The comparisons made for mass dispersion indicate that it is applicable to $(Re_p) > 100$. As it stands, the model is applicable to a bed packed with spherical or cylindrical pellets but not applicable to irregularly shaped pellets such as Rachig rings. Further work would be required to deal with irregularly shaped pellets. At high tube to pellet diameter ratios, say $D_t/d_p > 50$ as the comparisons for mass dispersion indicate, both Fickian and alternating flow models could describe well the observed dispersion behavior.

Notation

a = constants Eq. 27
$a^i_{j,k}$ = heat transfer area per unit length between jth and kth radial plugs, L
A = concentration vector for A half-cell, Eq. 13
A_i = void cross-sectional area of the ith radial plug, L^2
A_t = total tube cross-sectional area, L^2
B = concentration vector for B half-cell, Eq. 13
C = concentration, M/L^3
C_p = fluid heat capacity, $q/m \cdot \theta$
d = cylindrical pellet diameter, L
d_i = delay time in ith radial plug, Eq. 20
d_p = pellet diameter
D_a = axial dispersion coefficient, L^2/t
D_r = radial dispersion coefficient, L^2/t
D_t = tube diameter, L
f = friction factor
g_c = units conversion factor (e.g., 32.2 ft · lbm/lbf · s^2)
G = mass velocity, $M/L^2 \cdot \theta$
h_p = pellet film coefficient, $q/L^2 \cdot t \cdot \theta$
h_w = wall film coefficient, $q/L^2 \cdot t - \theta$
H = hydraulic resistance, Eq. 5
K = number of void plugs in a half-cell, $K = N_{rad}/2$
ℓ = cylindrical pellet length, L
L = length over which pressure drop occurs, L
n = axial cell number
N = total number of radial void plugs in a repeating cell
N_{axial} = total number of repeating axial cells
N_{rad} = same as N
ΔP = pressure drop, $M/L \cdot t^2$
Pe = Peclet number, proportional to $1/D_a$ or $1/Dr$
Q = volumetric flow rate, L^3/t
Q_i = flow rate through ith void radial plug, L^3/t
r = radial coordinate; has dimensions of L in Eq. 1, elsewhere scaled by $D_t/2$
$r_{i,j}$ = (i,j)th element of R
R = A-to-B mixing matrix, Eqs. 12, 15, 16
Re = Reynolds number
R_h = hydraulic radius, L
R_t = tube radius, L
s = Laplace transform variable
$s_{i,j}$ = (i,j)th element of S
S = B-to-A mixing matrix, Eqs. 11, 14, 17
S_p = external pellet surface area, L^2
t = solid temperature, θ
T = Fluid temperature, θ
T_{wall} = wall temperature, θ
U = velocity, L/t
v = velocity, L/t
V_p = pellet volume, L^3
W = weighting factor, Eqs. 6–8
x = radial distance in from tube wall, Eq. 27; units of d_p
z = axial coordinate, L
Z_t = total bed length, L
Z_c = length of one (A/B) repeating cell, L

Greek letters

β = proportionality constant, Eq. 5
γ = shape factor, =1.0 for spheres, =1.33 for cylinders
δ = tube roughness, L
ϵ = void fraction, L^3/L^3
θ_A = delay matrix, A half-cell
θ_B = delay matrix, B half-cell
τ = average bed holdup time, t
ρ = fluid density, M/L^3
λ = fluid thermal conductivity of $q/L \cdot t \cdot \theta$
λ_s = thermal conductivity of solid pellet material, $q/L \cdot t \cdot \theta$

Subscripts

a = radially averaged value
b = overall bed value
c = at bed centerline
e = effective
h = hydraulic
hi = upper value, Eq. 30
lo = lower value, Eq. 30
p = based on pellet diameter
s = solid
t = total, except with D_t
w = wall

Units

L = length
M = mass
q = heat, e.g., cal
t = time
θ = temperature

Appendix: Summary of AFM Equations

Determine ϵ_b:

Experiment or Leva-Grummer (1947a, b) correlation

Determine ϵ_{bulk}:

ϵ_{bulk}, Eqs. 25 to 27, to satisfy ϵ_b [$\epsilon_b = 2\int_0^1 r\epsilon(r)dr$]

Determine radial plugs:

$N_{rad} = (D_t/d_p)/0.816$ (round-up to next even integer) Evenly spaced at $\Delta r = D_t/d_p(1/N_{rad})$ Intermediate for A or B half-cell by Eq. 30.

Determine number:

$N_{axial} = Z_t/1.632d_p$ of axial cells.

Hydraulic resistance:

$$\frac{1}{H_i} = \beta A_i (Rh_i)^2 \quad Re_p < 150$$

$$= \beta A_i (Rh_i)^{1/2} \quad Re_p > 150$$

Flow division:

$$A \text{ half-cell } \frac{Q_i}{Q_t} = \frac{\frac{1}{H_i}}{\Sigma \frac{1}{H_i}} \quad i = 2, 4, \ldots, N$$

$$B \text{ half-cell } \frac{Q_i}{Q_t} = (1 - W_{i+2}) \frac{Q_{i+1}}{Q_t} + W_i \frac{Q_{i-1}}{Q_t}$$

$$i = 1, 3, \ldots, N-1$$

$$W_i = \frac{\frac{1}{H_i}}{\frac{1}{H_i} + \frac{1}{H_{i-2}}} \quad i = 1, 2, 3, \ldots, N$$

Steady state solution:

$\boldsymbol{A}_n = (\boldsymbol{SR})^{n-1} C_{in}$

$\boldsymbol{B}_n = \boldsymbol{RA}_n$, up to $n = N_{axial}$ (matrices defined in Eqs. 13–17)

Determine velocity profile:

$$\frac{U_i}{U_b} = \epsilon_b \left(\frac{Q_i}{Q_t}\right) \Big/ \left(\frac{A_i}{A_t}\right)$$

Determine delay-time profile:

$$\tau_i/\tau = A_i/A_t \Big/ \left(2N_{axial}\epsilon_b \frac{Q_i}{Q_t}\right)$$

Transient solution:

$(\boldsymbol{A}_{in})_n = (\boldsymbol{S\theta_B R\theta_A})^{n-1} C_{in}/s$

$(\boldsymbol{B}_{out})_n = \boldsymbol{\theta_B R\theta_A}(\boldsymbol{A}_{in})_n$, up to $n = N_{axial}$

θ_A, θ_B defined in Eq. 20

Literature cited

Aris, R., and N. R. Amundson, "Some Remarks on Longitudinal Mixing or Diffusion in Fixed Beds," *AIChE J.*, **3**, 280 (1957).

Baron, T., "Generalized Graphical Method for the Design of Fixed-Bed Catalytic Reactors," *Chem. Eng. Prog.*, **4**, 118 (1952).

Bennett, C. H., "Serially Deposited Amorphous Aggregates of Hard Spheres," *J. Appl. Phys.*, **43**, 2727 (1972).

Bennett, C. O., and J. E. Myers, *Momentum, Heat and Mass Transfer*, 3rd ed., McGraw-Hill, New York (1982).

Bird, R. B., W. E. Stewart, and E. N. Lightfoot, *Transport Phenomena*, Wiley, New York (1960).

Bischoff, K. B., and E. A. McCracken, "Tracer Tests in Flow Systems," *Ind. Eng. Chem.*, **58**, 18 (1966).

Buffham, B. A., "The Effects of Intrasolid Resistance and Axial Mixing on Transient Exchange in Packed Beds and the Unified Time Delay Model," *Chem. Eng.*, **2**, 71 (1971).

Cairns, E. J., and J. M. Prausnitz, "Longitudinal Mixing in Packed Beds," *Chem. Eng., Sci.*, **12**, 20 (1960).

Carberry, J. J., *Chemical and Catalytic Reaction Engineering*, McGraw-Hill, New York (1976).

Coberly, C. A., and W. A. Marshall, "Temperature Gradients in Gas Streams Flowing through Fixed Granular Beds," *Chem. Eng. Prog.*, **47**, 141 (1951).

Cohen, Y., and A. B. Metzner, "Wall Effects in Laminar Flow of Fluids through Packed Beds," *AIChE J.*, **27**, 705 (1981).

Danckwerts, P. V., "Continuous-Flow Systems Distribution of Residence Times," *Chem. Eng. Sci.*, **2**, 1 (1953).

Daugherty, R. L., and J. B. Franzini, *Fluid Mechanics with Engineering Applications*, McGraw-Hill, New York (1977).

Deans, H. A., and L. Lapidus, "A Computational Model for Predicting and Correlating the Behavior of Fixed-Bed Reactors," *AIChE J.*, **6**, 656 (1960).

Fahien, R. W., and J. M. Smith, "Mass Transfer in Packed Beds," *AIChE J.*, **1**, 28 (1955).

Froment, G. F., "Fixed Bed Catalytic Rector—Current Design Status," *Ind. Eng. Chem.*, **59**, 18 (1967).

Greenkorn, R. A., and D. P. Kessler, *Transfer Operations*. McGraw-Hill, New York (1972).

Gunn, D. J., "Theory of Axial and Radial Dispersion in Packed Beds," *Trans. Inst. Chem. Eng.*, **47**, T351 (1969).

Gunn, D. J., and C. Pryce, "Dispersion in Packed Beds," *Trans. Inst. Chem. Eng.*, **47**, T341 (1969).

Hiby, J. W., "Longitudinal and Transverse Mixing During Single-Phase Flow through Granular Beds," *Interaction between Fluids and Particles*, Inst. Chem. Eng., London, 312 (1963).

Hinduja, M. J., "A Non-Fickian Model for Dispersion in Packed Beds," Ph.D. Thesis, Rice Univ. (1977).

Hinduja, M. J., S. Sundaresan, and R. Jackson, "A Crossflow Model of Dispersion in Packed-Bed Reactors," *AIChE J.*, **26**, 274 (1980).

Jacques, G. L., and T. Vermeulen, *Longitudinal Dispersion in Solvent-Extraction Columns: Peclet Numbers for Ordered and Random Packings*, Report UCRL-8029, U.S. Atomic Energy Commission (1957).

Klingman, K. J., "Alternating Flow Model for Dispersion in Packed Beds," Ph.D. Thesis, Univ. Florida (1985).

Kubo, K., T. Aratani, A. Mishima, and T. Yano, "Mutual Relation between the Streamlines and the Residence Time Curve in Orderly Bead-Packed Beds," *Chem. Eng. J.*, **18**, 209 (1979).

Latinen, G. A., *Mechanisms of Fluid-Phase Mixing in Fixed and Fluidized Beds of Uniformly Sized Spherical Particles*, Ph.D. Thesis, Princeton Univ. (1954).

Lerou, J. J., and G. F. Froment, "Velocity, Temperature and Conversion Profiles in Fixed-Bed Catalytic Reactors," *Chem. Eng. Sci.*, **32**, 853 (1977).

Leva, M., "Heat Transfer to Gases through Packed Tubes; General Correlation for Smooth Spherical Particles," *Ind. Eng. Chem.*, **39**, 357 (July, 1947).

Leva, M., and M. Grummer, "Pressure Drop through Packed Tubes. II: Effect of Surface Roughness," *Chem. Eng. Prog.*, **43**, 633 (Nov. 1947).

———, "Pressure Drop through Packed Tubes, III: Prediction of Voids Variations," *Chem. Eng. Prog.*, **43**, 713 (Dec. 1947).

———, "Heat Transfer to Gases through Packed Tubes. Effect of Particle Characteristics," *Ind. Eng. Chem.*, **40**, 415 (Mar. 1948).

Levenspiel, O., *Chemical Reaction Engineering*, Wiley, New York (1962).

Levenspiel, O., and T. J. Fitzgerald, "A Warning on the Misuse of the Dispersion Model," *Chem. Eng. Sci.*, **38**, 489 (1983).

Lippert, E., and P. Schneider, "Combined Isothermal Diffusion and Forced Flow of a Binary Gaseous Mixture," *Chem. Eng. Commun.*, **3**, 65 (1979).

Marivoet, J., P. Teodoroiu, and S. J. Wajc, "Porosity, Velocity and Temperature Profiles in Cylindrical Packed Beds," *Chem. Eng. Sci.*, **29**, 1836 (1974).

McCabe, W. L., and J. C. Smith, *Unit Operations of Chemical Engineering*, 3rd ed., McGraw-Hill, New York (1976).
Ouchiyama, N., and T. Tanaka, "Porosity Estimation for Random Packings of Spherical Particles," *Ind. Eng. Chem. Fundam.*, **23,** 490 (1984).
Ranz, W. E., and W. R. Marshall, Jr., *Chem. Eng. Prog.*, **48,** 141, 173 (1952).
Ridgway, K., and K. J. Tarbuck, "Voidage Fluctuations in Randomly Packed Beds of Spheres Adjacent to a Containing Wall," *Chem. Eng. Sci.*, **23,** 1147 (1968).
Roblee, L. H., R. M. Baird, and J. W. Tierney, "Radical Profile Variations in Packed Beds," *AIChE J.*, **4,** 460 (1958).
Schertz, W. W., and K. B. Bischoff, "Thermal and Material Transport in Nonisothermal Packed Beds," *AIChE J.*, **15,** 597 (1969).
Schmalzer, D. K., and H. E. Hoelscher, "A Stochastic Model of Packed-Bed Mixing and Mass Transfer," *AIChE J.*, **17,** 104 (1971).
Schwartz, C. E., and J. M. Smith, "Flow Distribution in Packed Beds," *Ind. Eng. Chem.*, **45,** 1209 (1953).
Sherwood, T. K., and R. L. Pigford, *Adsorption and Extraction*, 2nd. ed., McGraw-Hill, New York, 970 (1952).
Stanek, V., and V. Eckert, "A Study of the Area Porosity Profiles in a Bed of Equal-Diameter Spheres Confined by a Plane," *Chem. Eng. Sci.*, 34, 933 (1979).
Sundaresan, S., N. R. Amundson, and R. Aris, "Observation on Fixed-Bed Dispersion Models: The Role of the Interstitial Fluid," *AIChE J.*, **26,** 529 (1980).
Vortmeyer, D., and J. Schuster, "Evaluation of Steady Flow Profiles in Rectangular and Circular Packed Beds by a Variational Method," *Chem. Eng. Sci.*, **38,** 1691 (1983).
Vortmeyer, D., and R. P. Winter, "On the Validity Limits of Packed-Bed Reactor Contiuum Models with Respect to Tube-to-Particle Diameter Ratio," *Chem. Eng. Sci.*, **39,** 1430 (1984).
Wen, C. Y., and L. T. Fan, *Models for Flow Systems and Chemical Reactors*. Dekker, New York (1975).
Yagi, S., and N. Wakao, "Heat and Mass Transfer from Wall to Fluid in Packed Beds," *AIChE J.*, **5,** 79 (1959).

Manuscript received Sept. 20, 1985 and Nov. 21, 1985 in two parts, and revision received July 24, 1986.